Article

Neuron

Nucleus to Synapse Nesprin1 Railroad Tracks Direct Synapse Maturation through RNA Localization

Highlights

- Nesprin1 forms actin-based railroad tracks from nucleus to synaptic boutons
- Nesprin1 is required for postsynaptic RNA localization and new bouton formation
- Nesprin1 function depends on unconventional Myosin, Myo1D
- We provide a mechanism for directed postsynaptic maturation via RNA localization

Authors

Mary Packard, Vahbiz Jokhi, ..., James Ashley, Vivian Budnik

Correspondence

vivian.budnik@umassmed.edu

In Brief

Packard et al. demonstrate that at the *Drosophila* NMJ, the nuclear associated protein, Nesprin1, forms long F-actin-containing striated filaments (railroad tracks) that connect the nucleus to nascent synaptic boutons. Nesprin1 railroad tracks are required for proper localization of postsynaptic RNAs and activity-dependent synaptic bouton formation in an unconventional myosin, Myo1D-dependent manner.

Packard et al., 2015, Neuron *86*, 1015–1028
May 20, 2015
http://dx.doi.org/10.1016/j.neuron.2015.04.006

CellPress

Neuron
Article

Nucleus to Synapse Nesprin1 Railroad Tracks Direct Synapse Maturation through RNA Localization

Mary Packard,[1,2] Vahbiz Jokhi,[1,2] Baojin Ding,[1] Catalina Ruiz-Cañada,[1] James Ashley,[1] and Vivian Budnik[1,*]
[1]Department of Neurobiology, University of Massachusetts Medical School, 364 Plantation Street, Worcester, MA 01452, USA
[2]Co-first author
*Correspondence: vivian.budnik@umassmed.edu
http://dx.doi.org/10.1016/j.neuron.2015.04.006

SUMMARY

An important mechanism underlying synapse development and plasticity is the localization of mRNAs that travel from the nucleus to synaptic sites. Here we demonstrate that the giant nuclear-associated Nesprin1 (dNesp1) forms striated F-actin-based filaments, which we dubbed "railroad tracks," that span from muscle nuclei to postsynaptic sites at the neuromuscular junction in *Drosophila*. These railroad tracks specifically wrap around immature boutons formed during development and in response to electrical activity. In the absence of dNesp1, mRNAs normally localized at postsynaptic sites are lacking and synaptic maturation is inhibited. This dNesp1 function does not depend on direct association of dNesp1 isoforms with the nuclear envelope. We also show that dNesp1 functions with an unconventional myosin, Myo1D, and that both dNesp1 and Myo1D are mutually required for their localization to immature boutons. These studies unravel a novel pathway directing the transport of mRNAs from the nucleus to postsynaptic sites during synaptic maturation.

INTRODUCTION

A crucial property of synaptic connections is their ability to change, which is thought to be at the core of adaptive processes, such as learning and memory and the refinement of connectivity (Mayford et al., 2012). A key feature of long-term changes in synaptic structure and function is the requirement for new protein synthesis (Mayford et al., 2012). In hippocampal neurons, ribonucleoprotein (RNP) granules are transported to the base of dendritic spines, and following plasticity-eliciting stimuli, result in RNP translocation to activated spines and induction of protein synthesis (Wang et al., 2010).

An important, yet poorly understood question is: How are RNPs directed to their precise destinations once they exit the nucleus? Studies in several systems provide evidence for directed trafficking of RNPs by binding to kinesin and dynein motors, thus supporting a role for microtubules in this process (Doyle and Kiebler, 2011; Medioni et al., 2012). However, studies also implicate actin filaments or actin-based motors, such as MyosinV/Didium, in the translocation of RNPs to dendritic spines or the posterior pole of the *Drosophila* oocyte (Doyle and Kiebler, 2011; Medioni et al., 2012). In the oocyte, the precise posterior localization of *oskar* mRNA, required to establish the anterior-posterior axis, requires both the activities of microtubules and actin-based motors. In this process MyosinV/Didium interacts with Kinesin heavy chain (Krauss et al., 2009), suggesting an interplay between the actin and microtubule cytoskeleton. It is proposed that microtubules could mediate long-range movements of RNPs from the nucleus to the periphery, but that precise localization of RNPs requires short-range interactions between RNPs and the actin-based cytoskeleton. However, these long versus short-range interactions are still ill defined.

To determine a potential role of the actin cytoskeleton in the postsynaptic localization of RNPs, we focused on the actin-binding protein MSP300/*Drosophila* Nesprin-1 (dNesp1; also known as Syne1), a component of the LInker of Nucleoskeleton and Cytoskeleton (LINC) complex (Kim et al., 2015; Volk, 1992). The LINC complex links the nuclear cytoskeleton with the actin-based cytoplasmic cytoskeleton. dNesp1 is a giant transmembrane protein of the spectrin superfamily (Rajgor and Shanahan, 2013), which is associated with a variety of musculoskeletal disorders, such as X-linked Emery-Dreifuss muscular dystrophy (EDMD), movement disorders such as autosomal recessive cerebellar ataxia type 1 (ARCA1), bipolar disorder, and it is a risk gene for schizophrenia and autism (Rajgor and Shanahan, 2013; Shinozaki and Potash, 2014). The largest isoform(s) of dNesp1 is embedded in the outer nuclear membrane (ONM) via its transmembrane domain. The C-terminal tail, containing a Klarsicht/Anc1/Syne Homology (KASH) domain, faces the nuclear intermembrane space (also referred as to the perinuclear space) between the ONM and the inner nuclear membrane (INM) and interacts with the INM Sad1/Unc84 (SUN) domain-containing proteins, thus connecting ONM and INM proteins. Its giant N-terminal domain faces the cytoplasm and contains multiple spectrin-type repeats as well as two calponin actin-binding domains. However, other dNesp1 isoforms lack the KASH domain and thus likely are not directly linked to the nuclear envelope.

At the mammalian neuromuscular junction (NMJ) Nesp1, is involved in interactions with the acetylcholine receptor (AChR) clustering molecule muscle-specific kinase (MuSK) (Apel et al., 2000). In the central nervous system CPG2, an isoform of Syne1, participates in the trafficking of glutamate receptors (GluRs) (Cottrell et al., 2004). Studies in *Drosophila* and mice

show that Nesp1 is required for normal nuclear localization in muscle cells (Volk, 2013; Zhang et al., 2010) and the integrity of muscle cell insertion sites into the cuticle (Volk, 1992). Recently, reports suggest that dNesp1 isoforms lacking the KASH domain are also required for normal *Drosophila* larval locomotion, selective localization of GluRIIA and synaptic function at the NMJ, independent of its nuclear localization role (Morel et al., 2014). However, its potential involvement in the localization of synaptic mRNAs has not been investigated.

Here we report that interfering with dNesp1 isoforms at the *Drosophila* NMJ disrupts the postsynaptic localization of mRNAs in muscle, and thus the localization of the proteins encoded by these mRNAs at the postsynaptic region. In addition, mutations in *dnesp1* alter synapse development and activity-dependent plasticity. In these mutants, mRNAs accumulate in the cytoplasm at the nuclear periphery, suggesting that the defect likely originates from abnormal transport of these mRNAs to synaptic sites and not from the nuclear export of these mRNAs. Strikingly in wild-type muscles, dNesp1 protein is organized into long striated filaments, dubbed "railroad tracks," which extend all the way from the nucleus to the periphery of the NMJ. dNesp1 railroad tracks are the first postsynaptic elements found to associate specifically with immature synaptic boutons formed during NMJ expansion or upon spaced stimulation. We show that dNesp1 binds to a synaptically localized RNA. In addition, dNesp1 colocalizes and cosediments with F-actin, confirming its relationship with the actin cytoskeleton. Furthermore, its exclusive localization around nascent synaptic boutons is similar to the distribution of the unconventional actin motor, Myo31DF, the *Drosophila* ortholog of human Myo1D. Null mutations in *myo31DF* mimic the phenotypes of the severe hypomorphic *dnesp1*^{sZ75} mutant, and both dNesp1 and Myo31DF are required for each other's localization. These studies unravel a novel filamentous network connecting the nucleus to nascent synaptic boutons, and this network functions with actin motors for proper localization of postsynaptic RNPs.

RESULTS

dNesp1 Is Required for Normal mRNA Localization at the NMJ

To determine a potential role of dNesp1 in the postsynaptic localization of mRNAs, we carried out fluorescence in situ hybridization (FISH) with probes to mRNAs previously found enriched at the larval NMJ. *Drosophila* larval NMJs are composed of synaptic boutons organized as beaded strings (Figure S1A). These NMJs innervate identified muscles of the body wall in a stereotypic manner, making comparisons across animals and genotypes straightforward. Synaptic boutons contain multiple glutamate release sites, and the entire presynaptic arbor can be selectively labeled with antibodies to HRP, which crossreact with neuronal carbohydrate epitopes (Jan and Jan, 1982) (Figure S1A). At the postsynaptic muscle region, synaptic boutons are apposed by the postsynaptic membrane containing GluR clusters in register with presynaptic active zones. Surrounding GluR clusters is the subsynaptic reticulum (SSR) a highly folded membrane structure derived from the muscle plasma membrane (Guan et al., 1996). This postsynaptic SSR is strongly labeled by antibodies to Discs-Large (Dlg) a scaffolding protein of the PSD95 family (Lahey et al., 1994) (Figure S1A).

In this study, we focused on transcripts encoding the PDZ-scaffolding proteins, Par6 and MAGI (Jokhi et al., 2013; Speese et al., 2012). As reported, in wild-type larvae *par6* and *magi* FISH signals were enriched at the postsynaptic region of the NMJ, outside the HRP-labeled presynaptic terminal (Figures 1A and 1C; Figure S1A). In contrast, in the severe hypomorphic mutant, *dnesp1*^{sZ75}, the NMJ FISH signal was markedly decreased (Figures 1B, 1D, and 1J). This reduction was specific to mutations in *dnesp1*, because the defect was completely rescued by a duplication of the *dnesp1* locus (Figure 1J). Other mRNAs not concentrated at the NMJ, such as *dlg*, were not affected in *dnesp1*^{sZ75} mutants (Figure 1L).

The *dnesp1*^{sZ75} mutation introduces an early stop codon into the 12th exon of the *dnesp1* gene, thus predicting the truncation of 80% of the giant full-length protein (~1.5 MDa) and potentially generating truncated protein species of 260–300 kDa (Yu et al., 2006). dNesp1 immunoprecipitation from body wall muscle protein extracts using an antibody that recognizes nearly all dNesp1 isoforms (Volk, 1992) shows that the *dnesp1*^{sZ75} mutation eliminates all giant dNesp1 isoforms (above 1 MDa), although lower molecular mass species (below 300 kDa) are still observed at lower levels (Figure 1I). Thus, in the absence of giant dNesp1 isoforms, transcripts known to localize at the postsynaptic region are severely decreased.

The depletion of *par6* and *magi* mRNAs at the NMJ could be explained by abnormal *dnesp1* transcription, RNP packaging/RNA stability, defective nuclear export, or inappropriate transport of RNPs to the NMJ. To discern between these possibilities we examined the distribution of *par6* and *magi* transcripts within the nucleus and in the cytoplasm around the nucleus. Notably, the reduction of postsynaptic *par6* and *magi* mRNA in *dnesp1*^{sZ75} mutants was correlated with a 2-fold increase in FISH signal in the cytoplasm at the nuclear periphery (Figures 1M–1O). The increase in signal resulted from both an increase in the number of bright fluorescent punctae and a more diffuse signal and was completely rescued by a duplication of the *dnesp1* locus (Figure 1M–1P). Together with the data showing that levels of *par6* and *magi* RNA are decreased at postsynaptic sites, these observations raise the possibility that in *dnesp1*^{sZ75} mutants megaRNPs are exported normally from the nucleus but that their transport to postsynaptic sites might be disrupted. Consistent with this idea, the total levels of *par6* RNA in larval body wall muscles was not decreased in *dnesp1*^{sZ75} mutants as determined by real-time PCR (Figure 1Q), further suggesting that RNA stability is unlikely to be affected in the *dnesp1*^{sZ75} mutant. Similarly, the levels and distribution of Torsin at the nuclear envelope were normal (Figure S1B). Although we did observe a larger than normal number of nuclear Lamin C foci, we never observed abnormal megaRNP granules in the *dnesp1*^{sZ75} mutant as in the case of *torsin* mutants at the EM level (Jokhi et al., 2013) (not shown; n: 37 nuclei from 3 animals). In addition, the *par6* RNA levels were increased in the perinuclear region of the *dnesp1*^{sZ75} mutant, suggesting that *par6* nuclear export is not inhibited. Taken together, the most straightforward explanation for the decrease in FISH signal at the postsynaptic region is a defective RNA transport.

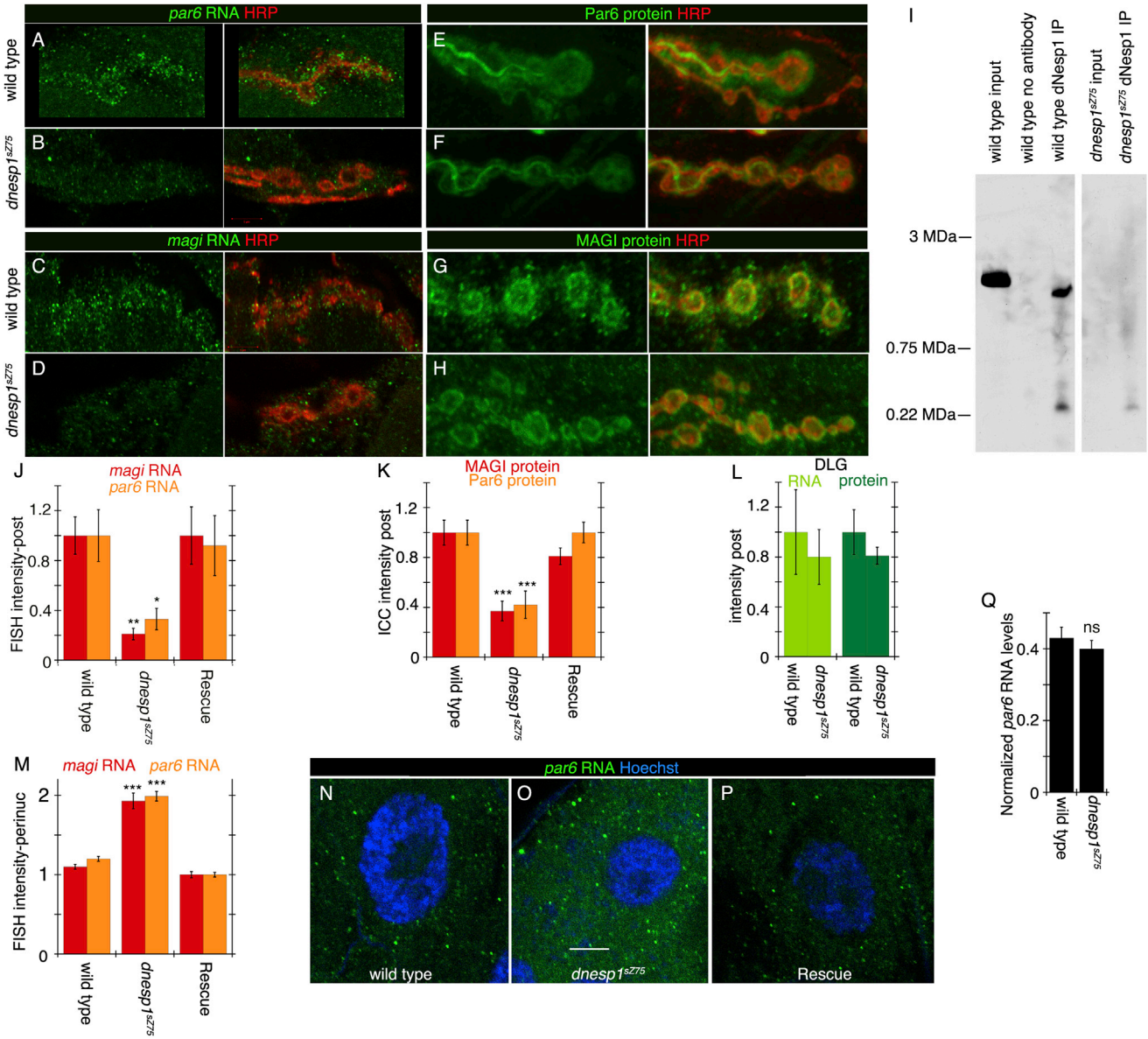

Figure 1. *magi* and *par6* mRNAs Are Depleted at the NMJ of *dnesp1*^{sZ75} Mutants

(A–D) Larval NMJs labeled with anti-HRP and FISH to (A), (B) a *par6* probe, and (C and D) a *magi* probe in (A) and (C) wild-type and (B) and (D) *dnesp1*^{sZ75} mutants.

(E–H) Larval NMJs labeled with anti-HRP and either (E), (F) anti-Par6 or (G) and (H) anti-MAGI in the indicated genotypes.

(I) Immunoprecipitation of dNesp1 in wild-type and *dnesp1*^{sZ75} mutants.

(J–L) Quantification of postsynaptic signal intensity normalized to wild-type control (see Experimental Procedures) for (J) *par6* and *magi* RNA. (K) Par6 and MAGI protein and (L) DLG RNA and protein, in wild-type, *dnesp1*^{sZ75}, and *dnesp1*^{sZ75} mutants containing two copies of a duplication of the *dnesp1* locus (rescue).

(M) Ratio of FISH signal (intensity:background) in the region surrounding the nucleus in the above genotypes.

(N–P) Muscle nuclei labeled with Hoechst, and FISH to *par6* in (N) wild-type, (O) *dnesp1*^{sZ75} mutants, and (P) rescue.

(Q) qPCR of *par6* mRNA from wild-type and *dnesp1*^{sZ75} mutants normalized to *ef1α48D*.

Calibration scale: (A–H): 4 μm; (N–P) 6 μm. Error bars represent ± SEM (*$p < 0.05$, **$p < 0.001$, ***$p < 0.0001$). Number of samples (animals:arbors/muscles): (J) 20:38,18:36, 10:20, 9:18, 10:20, 9:18; (K) 8:15, 8:16, 8:15, 8:16, 8:15, 8:16; (L) 9:18, 9:18, 9:18, 9:18; (M) 7:13, 7:14, 7:13, 6:12, 6:12, 6:12; (Q) 3. Images correspond to single confocal slices.

See also Figure S1.

A decline in the transport of *par6* and *magi* mRNA from the perinuclear area to the NMJ should be reflected in a decrease in the levels of postsynaptic Par6 and MAGI protein, which was tested using antibodies specific for these proteins (Jokhi et al., 2013; Ruiz-Canada et al., 2004). As with the FISH signal at the NMJ, we found that mutations in *dnesp1*^{sZ75} led to a substantial decrease in the levels of Par6 and MAGI immunoreactivity at the postsynaptic site, which was completely rescued

by a duplication of the *dnesp1* locus (Figures 1E–1H and 1K). Interestingly, an additional *dnesp1* mutation (*dnesp1*$^{\Delta KASH}$) lacking the C-terminal region, including the nuclear transmembrane domain and the KASH domain, a domain known to link dNesp1 to nuclear envelope proteins, showed no such alteration in Par6 protein localization (Figures S1C–S1E). Thus, interfering with giant *dnesp1* isoforms, but not deletion of the transmembrane and KASH domains, prevents normal transport of transcripts that are normally localized at the NMJ, and this defect interferes with normal postsynaptic protein composition.

dNesp1 Establishes a Long-Range Filamentous Network that Specifically Interacts with Nascent Boutons at the NMJ

We next determined how dNesp1 could participate in the transport of postsynaptic mRNAs to the NMJ. We first examined the distribution of dNesp1 protein in wild-type body wall muscles using *Drosophila* anti-dNesp1 antibodies (Volk, 1992). As previously reported (Elhanany-Tamir et al., 2012), dNesp1 had a wide distribution in muscle cells, showing strong immunoreactivity at Z-bands within the contractile apparatus (Figure 2A) and throughout the muscle cell cortical region. dNesp1 immunoreactivity also outlined the nucleus, but was excluded from the nucleoplasm (Figures 2A and 2B). We also observed long dNesp1 positive filaments that fully extended all the way from the nuclear periphery to distant regions of the muscle cell cortex, including regions neighboring the NMJ (Figures 2B and 2G; arrowheads). Similar filaments were observed in *dnesp1*$^{\Delta KASH}$ (Figure 2C, arrowheads), suggesting that these filaments do not depend on direct interactions between dNesp1 and the nuclear envelope. These filaments, similar to the filaments observed at Z-bands had a striated appearance (Figure 2G; arrowheads), and thus we dubbed them "railroad tracks."

Although extending toward the NMJ, dNesp1 was largely excluded from the majority of synaptic boutons at the NMJ (Figure 2A). However, dNesp1 signal was often observed surrounding a very small number of synaptic boutons (Figure 2A; arrows). This NMJ dNesp1 signal was examined in conjunction with pre- and postsynaptic markers (anti-HRP to label the presynaptic compartment and anti-DLG to label the postsynaptic NMJ region; Figure S1A). Strikingly, boutons that were surrounded by dNesp1 immunoreactivity were devoid of Dlg signal and thus correspond to "ghost" boutons (Figures 2D, 2E, and 2I). Previous studies show that during larval development, presynaptic boutons are first formed from an expanding NMJ arbor, and that the recruitment of their postsynaptic proteins occurs after bouton extension (Ataman et al., 2008). Thus, ghost boutons correspond to a transient, immature synaptic bouton developmental stage, which lacks the post-synaptic apparatus. The filamentous postsynaptic localization of dNesp1 at ghost boutons was also demonstrated using STimulated Emission Depletion (STED) microscopy (Figure 2F). Quantification of the association of dNesp1 with ghost boutons revealed that 97% (from 42 ghost boutons) of ghost boutons were surrounded by dNesp1. Figure 2J shows relative intensities of dNesp1, HRP, and Dlg at the peak of HRP intensity (±0.4 μm; bouton border) in mature and ghost boutons, showing that in contrast to mature boutons, ghost boutons are associated with dNesp1 and have minimal Dlg signal (Figures 2J and 2K).

dNesp1 immunoreactivity was specific because it was virtually eliminated in the *dnesp1*^{sZ75} severe hypomorphic mutant (Figure 2H). In addition, the localization of dNesp1 to ghost boutons was unaffected in the *dnesp1*$^{\Delta KASH}$ mutants (Figures S2A and S2B), suggesting that direct anchoring of dNesp1 to the nuclear envelope is not required for dNesp1 targeting to ghost boutons. This is consistent with the observation that the levels of postsynaptic Par6 were not affected in the *dnesp1*$^{\Delta KASH}$ mutants (Figures S1D–S1F). To our knowledge, dNesp1 is the first identified protein that specifically marks these immature boutons, raising the possibility that dNesp1 is involved in the first stages of synaptic bouton maturation. Furthermore, the lack of postsynaptically localized transcripts in the severe hypomorphic mutant, combined with the accumulation of these transcripts at the periphery of the nucleus, implicates dNesp1 railroad tracks in the transport of mRNAs required for the formation of postsynaptic structures.

To determine if dNesp1 could associate with RNAs, we immunoprecipitated dNesp1 from body wall muscle protein extracts and tested whether *par6* RNA co-precipitated with dNesp1 in wild-type and *dnesp1*^{sZ75} mutants. We found that *par6* RNA indeed co-precipitated with dNesp1 in wild-type (over 12-fold increase compared to no antibody control), and that the levels of *par6* coprecipitation was substantially reduced in *dnesp1*^{sZ75} mutants (~2-fold increase compared to no antibody control; Figure 2L; Figure S2C). The association between dNesp1 and *par6* RNA was specific because the negative control transcripts, *ef1α48D* and *rpL32,* co-precipitated with dNesp1 to a far lesser extent in both wild-type and *dnesp1*^{sZ75} mutants (Figure S2D).

In wild-type larvae, ghost boutons are observed infrequently presumably because they rapidly mature. However, previous studies show that ghost boutons are induced by spaced electrical stimulation paradigms based on motor nerve stimulation, activation of motorneuron-expressed Channelrhodopsin 2 (ChR2), or high K^+-induced depolarization (Ataman et al., 2008). To determine if dNesp1 associates with newly formed ghost boutons, we first used a spaced paradigm of five cycles of high K^+-induced depolarization, each separated by 15 min of rest, to induce ghost bouton formation. Then, preparations were fixed and triple-labeled with antibodies to HRP, DLG, and dNesp1. In unstimulated controls, ghost boutons were seldom observed (Figure 3A). However, in stimulated preparations, many ghost boutons that were surrounded by dNesp1 were formed (Figure 3B; see below for quantification of ghost boutons upon stimulation). These observations support the notion that dNesp1 is one of the earliest localized proteins at postsynaptic sites during synaptic bouton formation.

dNesp1 Function Is Required for Normal Synaptic Bouton Maturation and Activity-Dependent Plasticity

To determine the role of dNesp1 during synaptic bouton formation, we examined the NMJ in mature third-instar larvae in wild-type and *dnesp1*^{sZ75} mutants. We found that in *dnesp1*^{sZ75}, the number of synaptic boutons was markedly reduced (Figures 4A, 4C, and 4F). Furthermore, as in other mutants that prevent synaptic bouton maturation, NMJs from *dnesp1*^{sZ75} mutants

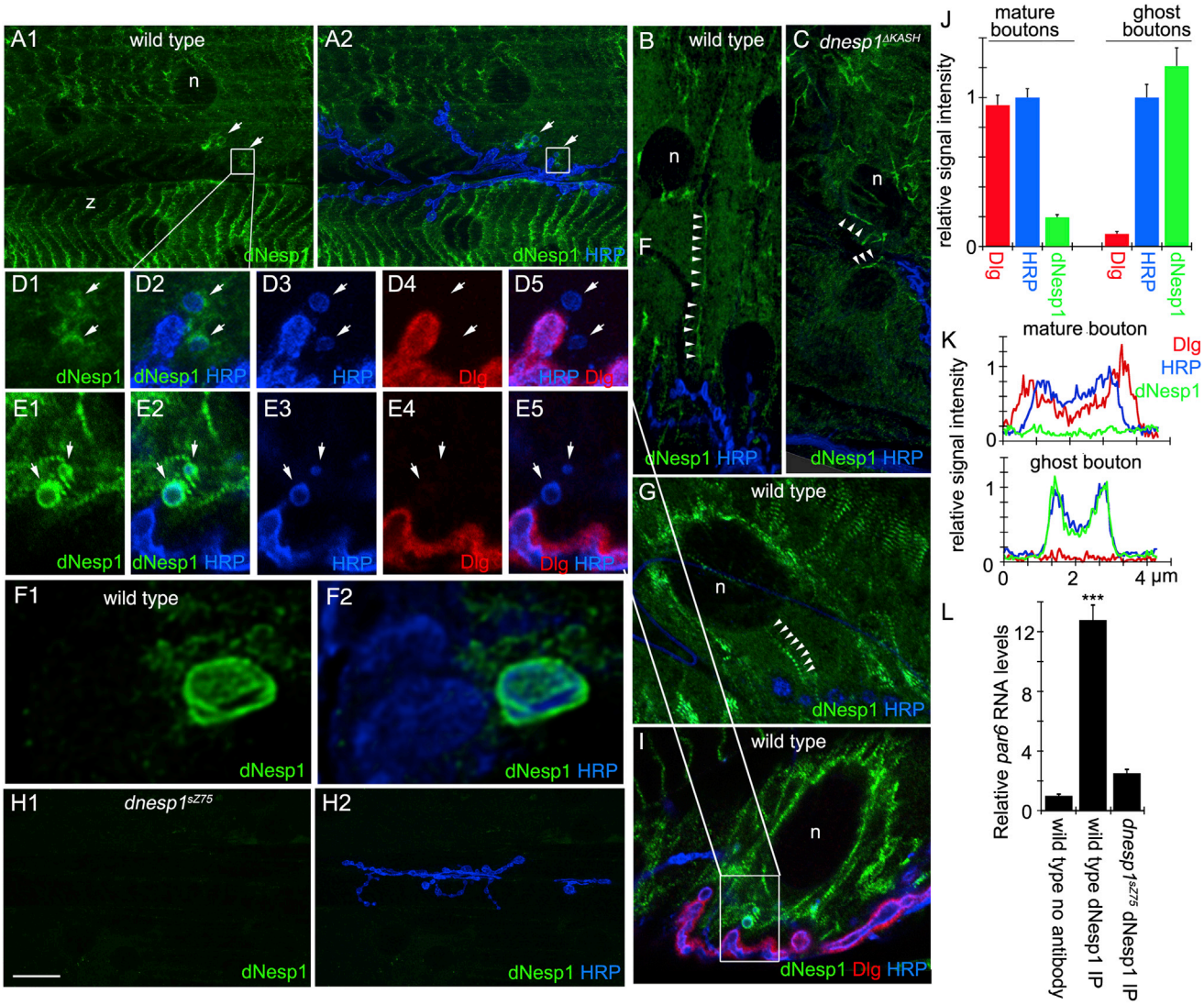

Figure 2. dNesp1 Railroad Tracks Specifically Wrap around Ghost Boutons

(A–I) Body wall muscles and NMJs labeled with anti-dNesp1, anti-HRP, and anti-DLG in (A), (B), (D)–(G), (I) wild-type; (C) *dnesp1*$^{\Delta KASH}$; and (H) *dnesp1*^{sZ75} mutants. Arrowheads point to dNesp1 railroad tracks; z, Z-line; n, nucleus. (D and E) High-magnification views of the regions marked by the boxes in (A) and (I), respectively) showing the presence of ghost boutons (arrows), which are labeled with anti-dNesp1 and anti-HRP, but not with anti-DLG. (F) STED image of a ghost bouton, showing dNesp1 label wrapping around a ghost bouton.

(J) Quantification of anti-DLG, anti-dNesp1, and anti-HRP signal at the bouton border (see Experimental Procedures; n = 6) normalized to HRP intensity.

(K) Representative relative signal intensity across the midline of a mature and a ghost bouton.

(L) Relative levels of *par6* RNA immunoprecipitated with dNesp1 as measured by real-time PCR (n = 3 biological replicates).

Calibration scale: (A–C, G–I) 10 μm; (D and E) 4 μm; (F) 2 μm. Number of samples in (J) is six boutons. Images represent single confocal slices. Error bars represent ± SEM (*p < 0.05, **p < 0.001, ***p < 0.0001).

See also Figure S2.

had a significant increase in the number of ghost boutons (Figures 4B, 4D, 4E, arrows, and 4G). These mutant phenotypes were specific because they were completely rescued by two copies of a duplication of the *dnesp1* locus (Figures 4F and 4G). Interestingly, *dnesp1*^{sZ75}/+ heterozygotes also showed an enhancement in the number of ghost boutons, which was on average more pronounced than *dnesp1*^{sZ75} homozygotes (Figure 4G). However, this difference between the *dnesp1*^{sZ75} homozygote and heterozygote was not statistically significant. The defect in the heterozygote was rescued by introducing one copy of the duplication of *dnesp1* (Figure 4G). Notably, no significant changes were observed in the number of synaptic boutons or ghost boutons in a *dnesp1* mutation deleting the C-terminal region, including the transmembrane and KASH domains, *dnesp1*$^{\Delta KASH}$ (Figures 4F and 4G). These results support a role for dNesp1 in synaptic maturation and suggest that this role is

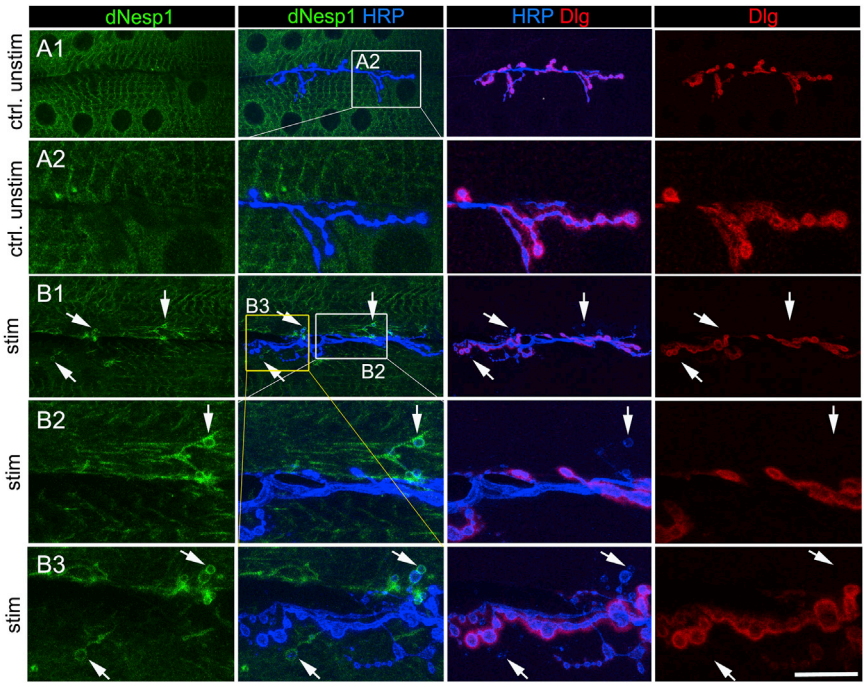

Figure 3. dNesp1 Is Localized to New Ghost Boutons Induced by Spaced Stimulation

(A and B) Wild-type NMJ arbors labeled with anti-dNesp1, anti-HRP, and anti-DLG in (A) unstimulated samples (box in A1 is shown at higher magnification in A2), and (B) samples subjected to high K^+ stimulation (boxes in B1 are shown at high magnification in B2 and B3), showing that activity-induced ghost boutons (arrows) are wrapped by dNesp1. Calibration scale: (A1 and B1) 50 μm; (A2, B2, and B3) 20 μm. Images represent single confocal slices. See Figure 5 for quantification.

independent of interactions between dNesp1 and nuclear envelope proteins.

We also determined whether dNesp1 functions in the postsynaptic muscle or presynaptic neuron during NMJ development because dNesp1 is expressed in both tissues (FlyBase: FBgn0261836; http://flybase.org/reports/FBgn0261836.html). In these experiments, we expressed dNesp1-RNAi either in neurons (using the neuronal elav-Gal4 driver) or muscles (using the muscle-specific C600-Gal4 driver; Figure S3) and quantified the number of synaptic boutons and ghost boutons in the third instar larval stage. Downregulating dNesp1 in neurons elicited a small but significant decrease in the number of synaptic boutons (Figure 4F). However, this decrease was not accompanied by an increase in the number of ghost boutons (Figure 4G). In contrast, the phenotype of the *dnesp1*^{sZ75} mutant was completely recapitulated by downregulating dNesp1 in muscles with respect to total bouton count (Figure 4F) and number of ghost boutons (Figure 4G). Thus, dNesp1 appears to function in both neurons and muscles, but its contribution to NMJ expansion is predominantly exerted by its function in muscle. This is consistent with our finding that maturation of ghost boutons requires a retrograde signal from muscle (Korkut et al., 2013).

We next determined if, in addition to a role in synaptic maturation, dNesp1 could be involved in rapid activity-dependent bouton formation. In these experiments, both wild-type and *dnesp1*^{sZ75} mutants were subjected to the spaced high K^+ stimulation paradigm. Interestingly, both wild-type controls and *dnesp1*^{sZ75} mutants were capable of generating new ghost boutons in response to spaced stimulation (Figures 5A–5D and 5I). However, the response of *dnesp1*^{sZ75} mutants was significantly reduced (Figure 5I), providing support for the notion that dNesp1 is required for bouton formation. We also determined the likely fate of ghost boutons over 8hrs after formation. In these experiments, intact (undissected) larvae expressing Channelrhodopsin2 (ChR2) in motor neurons were stimulated with blue light following our spaced protocol (Ataman et al., 2008). Then, larvae were dissected at 2 and 8 hr after the start of stimulation. Similar to K^+ stimulation, wild-type larvae exhibited a highly significant increase in the number of ghost boutons upon light stimulation (Figure 5J). At 8 hr, however, the number of ghost boutons was significantly decreased, suggesting that these newly formed boutons either matured or were eliminated (Figure 5J). In *dnesp1*^{sZ75} mutants, ChR2 activation by light also resulted in an increase in the number of ghost boutons, although significantly smaller than wild-type, consistent with the results with K^+ stimulation. Notably, however, these ghost boutons persisted even after 8 hr (Figure 5J). Together with the observations that *dnesp1*^{sZ75} mutants have significantly fewer mature boutons, and an accumulation of ghost boutons, these results suggest that in *dnesp1*^{sZ75} mutants newly formed boutons fail to mature.

dNesp1 Railroad Tracks Colocalize with F-Actin Filaments and dNesp1 Function Requires a Myosin 1 Actin Motor

The above observations suggest a role of dNesp1 railroad tracks in the transport of mRNAs required for postsynaptic development. As both F-actin and microtubules have been implicated in the transport of RNPs, we next determined if dNesp1 railroad tracks were associated with these cytoskeletal components. Labeling preparations with fluorescently conjugated phalloidin revealed that dNesp1 railroad tracks coincided with F-actin microfilaments (Figures 5E, 5G, and 5H). As with dNesp1, F-actin filaments had a striated organization and the striations were staggered with those of dNesp1 with a period of ~0.5 μm (Figures 5G and 5H). The association of dNesp1 and F-actin is consistent with previously published observations suggesting that dNesp1 cosediments with F-actin in both in mammals and *Drosophila* (Volk, 1992; Zhang et al., 2002), which was confirmed here for body wall muscle extracts (Figure S4). They are also consistent with the presence of two calponin actin-binding domains in dNesp1. In contrast, no colocalization was observed between dNesp1 railroad tracks and microtubules, which were labeled with an antibody to tyrosinated tubulin (Figure 5F).

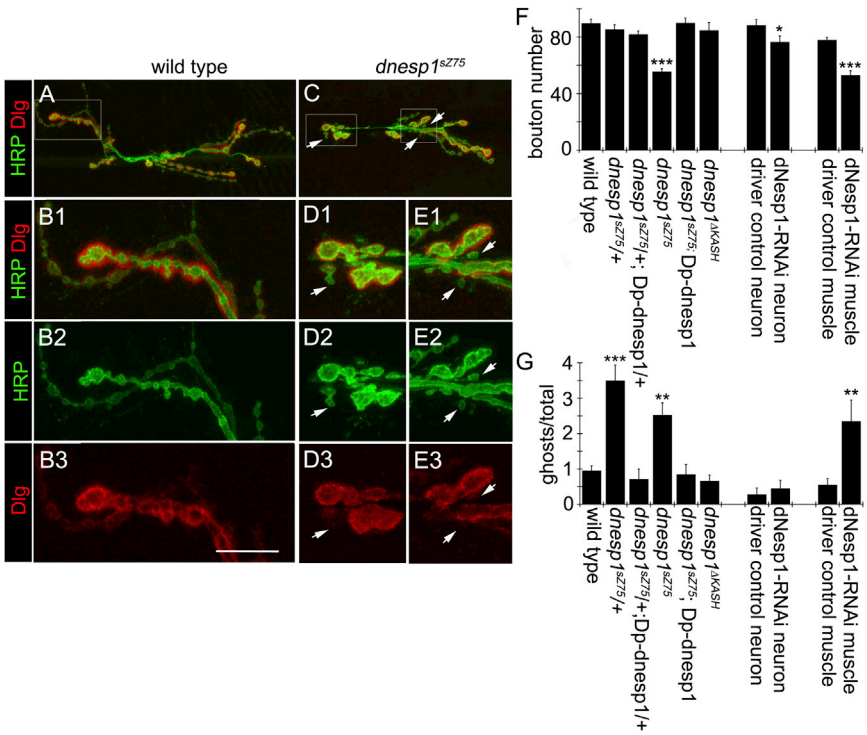

Figure 4. NMJ Expansion and Synaptic Bouton Maturation Depend on *dnesp1* but Are Independent from the KASH Domain

(A–E) Larval NMJs labeled with anti-HRP and anti-DLG shown at (A) and (C) low and at (B), (D), and (E) high magnification from (A) and (B) wild-type and (C)–(E) *dnesp1*^{sZ75} mutant. Arrows point to ghost boutons, which are devoid of DLG label.

(F and G) Quantification of (F) synaptic bouton number and (G) ghost bouton number (divided by total bouton number and normalized to wild-type controls) in the indicated genotypes.

Calibration scale: (A and C) 40 μm; (B, D, and E) 12 μm. Error bars represent ± SEM (*p < 0.05, **p < 0.001, ***p < 0.0001). Number of samples are (animals:arbors; from left to right) (F) 31:62, 28:56, 33:65, 23:45, 28:55, 12:24, 12:24, 12:24, 12:24, and 12:24; (G) 31:62, 28:56, 33:65, 23:46, 29:57, 12:24, 12:24, 12:24, 12:24, and 12:24. Images correspond to (A) and (C) a maximal intensity Z-stack projection, and (B) (D), and (E) single confocal slices.

See also Figure S3.

If dNesp1 railroad tracks serve to transport RNPs, then we predict that actin motors should be associated with dNesp1. We found that a member of the myosin1 family, Myo31DF, which is 53% identical to human Myo1D was highly enriched at ghost boutons, although it was also observed at low levels at the entire NMJ (Figure 6A). The immunoreactivity was specific as it was eliminated in the trans-allelic *myo31DF* mutant combination *myo31DF*^{K1}/*myo31DF*^{K2} (Figure 6B). As expected, ghost boutons labeled by Myo31DF were also labeled by anti-dNesp1 (Figure 6C). In the muscle cytoplasm, Myo31DF had a low intensity punctate appearance (Figure 6C). Unfortunately, optimal preservation of dNesp1 railroad tracks required fixation conditions different from those required to depict Myo31DF and although some of the Myo31DF puncta colocalized with dNesp1 railroad tracks (insets in Figure 6C), it was not possible to conclusively determine if Myo31DF was always associated with dNesp1 railroad tracks. Figure 6G shows the Pearson's colocalization index between dNesp1 and Myo31DF in the cytoplasm, at mature boutons, and at ghost boutons, showing near perfect colocalization at ghost boutons. Nevertheless, *myo31DF* null mutations not only mimicked the decrease in bouton number observed in *dnesp1*^{sZ75} hypomorphic mutants (Figure 6H), but also far surpassed *dnesp1*^{sZ75} mutants in ghost bouton accumulation (Figure 6I).

To determine the extent of the similarities between *dnesp1*^{sZ75} and *myo31DF* mutant phenotypes, we induced ghost bouton formation using the spaced stimulation protocol with high K^+-induced depolarization in wild-type and *myo31DF* mutants. As in *dnesp1*^{sZ75} mutants, *myo31DF* mutants showed a significant reduction in activity-dependent formation of ghost boutons (Figure 6J). Similarly, whereas in stimulated wild-type controls ghost boutons significantly decreased in number 8 hr after initiation of stimulation, in *myo31DF* mutants they remained unchanged at 8 hr (Figure 6J). Importantly, unlike wild-type controls (Figure 6D), in the absence of Myo31DF, dNesp1 failed to surround any of the ghost boutons induced upon stimulation (Figure 6E). Thus, Myo31DF is required for the proper extension of dNesp1 railroad tracks to nascent boutons.

The abnormal localization of dNesp1 in *myo31DF* mutants raised the question of whether dNesp1 had a similar role in Myo31DF localization. We found that in *dnesp1*^{sZ75} mutants, the distribution of Myo31DF was completely altered (Figure 6F). Instead of localizing at low levels at the NMJ and being enriched around ghost boutons, Myo31DF formed filaments in the muscle cortical region near the NMJ (Figure 6F) suggesting that Myo31DF and dNesp1 are mutually required for each other's localization. Taken together, the above results suggest that dNesp1 and Myo31DF function together in synaptic bouton formation and maturation. This hypothesis was tested by examining if *dnesp1* and *myo31DF* interacted genetically. Neither heterozygous *dnesp1*^{sZ75}/+ nor *myo31DF*/+ had a significant decrease in the number of boutons, but transheterozytotes *dnesp1*^{sZ75}/+, *myo31DF*/+ had a significant decrease (Figure 6K). Most strikingly, whereas *dnesp1*^{sZ75}/+ heterozygotes had a substantial increase in the number of ghost boutons, this phenotype was completely suppressed in the *dnesp1*^{sZ75}/+, *myo31DF*/+ transheterozygote (Figure 6L). These observations suggest that *dnesp1* and *myo31DF* interact genetically and that *myo31DF* is downstream of *dnesp1*.

Because in *myo31DF* mutants ghost boutons are no longer surrounded by dNesp1, we also expected that in these mutants *par6* and *magi* RNA transport to the NMJ should be severely inhibited. We found that indeed, both *par6* and *magi* transcripts were depleted from the NMJ (Figures 7A–7D and 7I). In addition,

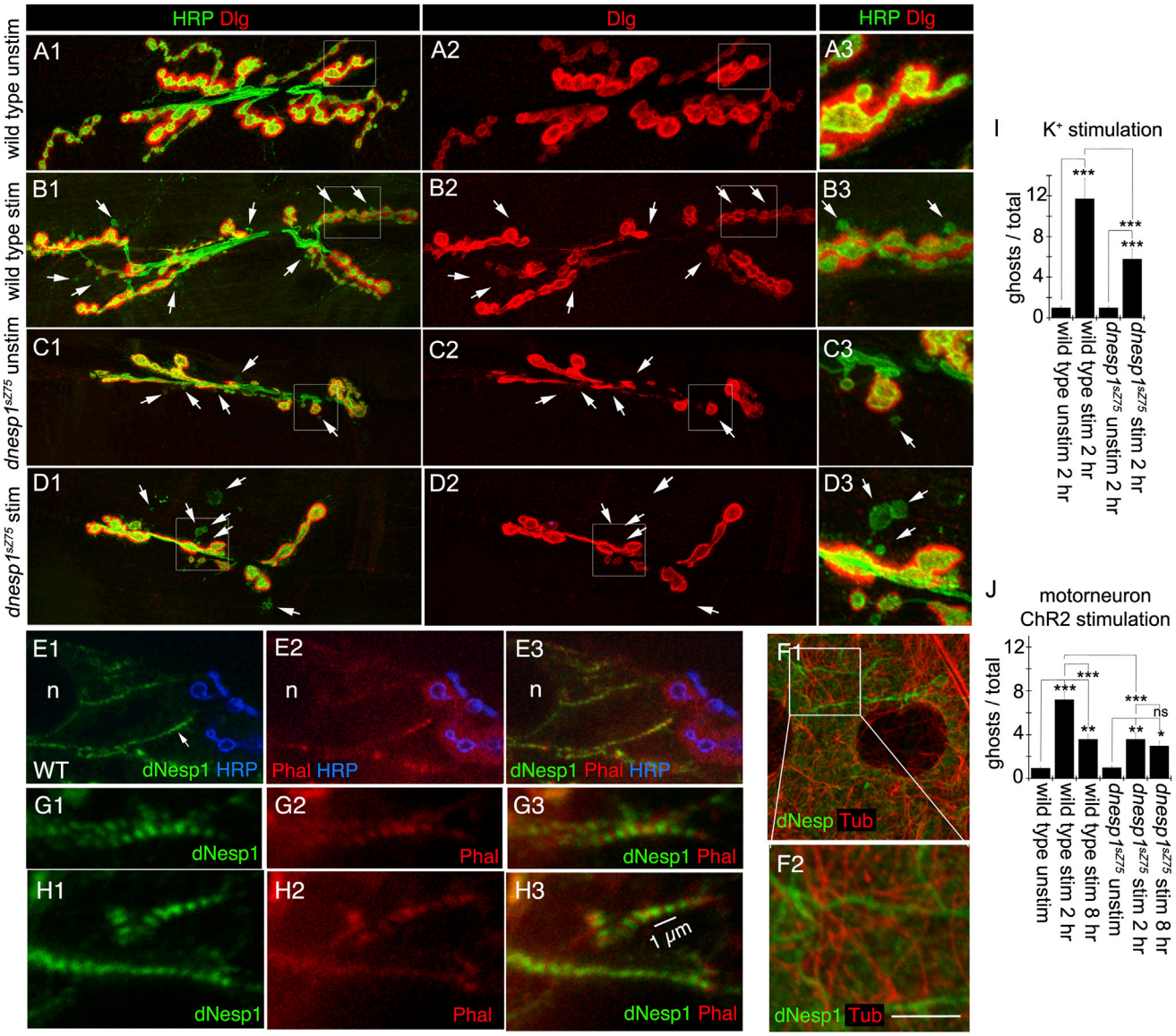

Figure 5. Mutations in *dnesp1* Alter Activity-Dependent Bouton Formation, and dNesp1 Railroad Tracks Contain F-Actin

(A–D) NMJ arbors labeled with anti-HRP and anti-DLG from (A) and (C) unstimulated controls and (B) and (D) body wall muscles subjected to high K^+ spaced stimulation, in (A) and (B) wild-type and (C) and (D) *dnesp1*^{sZ75} mutants. Arrows point to ghost boutons.

(E, G, and H) Larval body wall muscle labeled with anti-dNesp1, fluorescent phalloidin to mark F-actin, and anti-HRP showing that (E) long dNesp1 railroad tracks (arrow) spanning from the nucleus to the NMJ contain F-actin, and (G and H) that these railroad tracks are composed of staggered F-actin and dNesp1 striations.

(F) Larval body wall muscle labeled with anti-tubulin and dNesp1, showing that dNesp1 and microtubules are non-overlapping. Box in (F1) is shown at high magnification in (F2).

(I and J) Quantification of ghost bouton number (divided by total bouton number and normalized to wild-type controls) from animals stimulated with spaced (I) high K^+ or (J) Chr2 stimulation in the indicated genotypes showing that *dnesp1*^{sZ75} mutants have reduced activity-dependent induction of ghost boutons and synaptic bouton maturation.

Calibration scale: (A–D; images 1,2)18 μm; (A–D; image 3) 6 μm; (E) 7 μm, (F) 10 μm; and (G and H) 3 μm. Error bars represent ± SEM (*$p < 0.05$, **$p < 0.001$, ***$p < 0.0001$). Number of samples (animals:arbors; left to right): (I) 31:62, 33:65, 11:21, 11:22; (J) 30:59, 33:66, 28:56, 30:59, 19:37, 28:56. Images correspond to (A)–(D) maximal intensity Z stack projections and (E) and (F) single confocal slices. See also Figure S4.

there was a drastic reduction in postsynaptic Par6 and MAGI protein levels at the NMJ (Figures 7E–7H and 7J). Thus, dNesp1 and Myo31DF are mutually required for specific transcript localization.

DISCUSSION

mRNA localization and local translation are critical for the formation and plasticity of synaptic connections. However, the exact

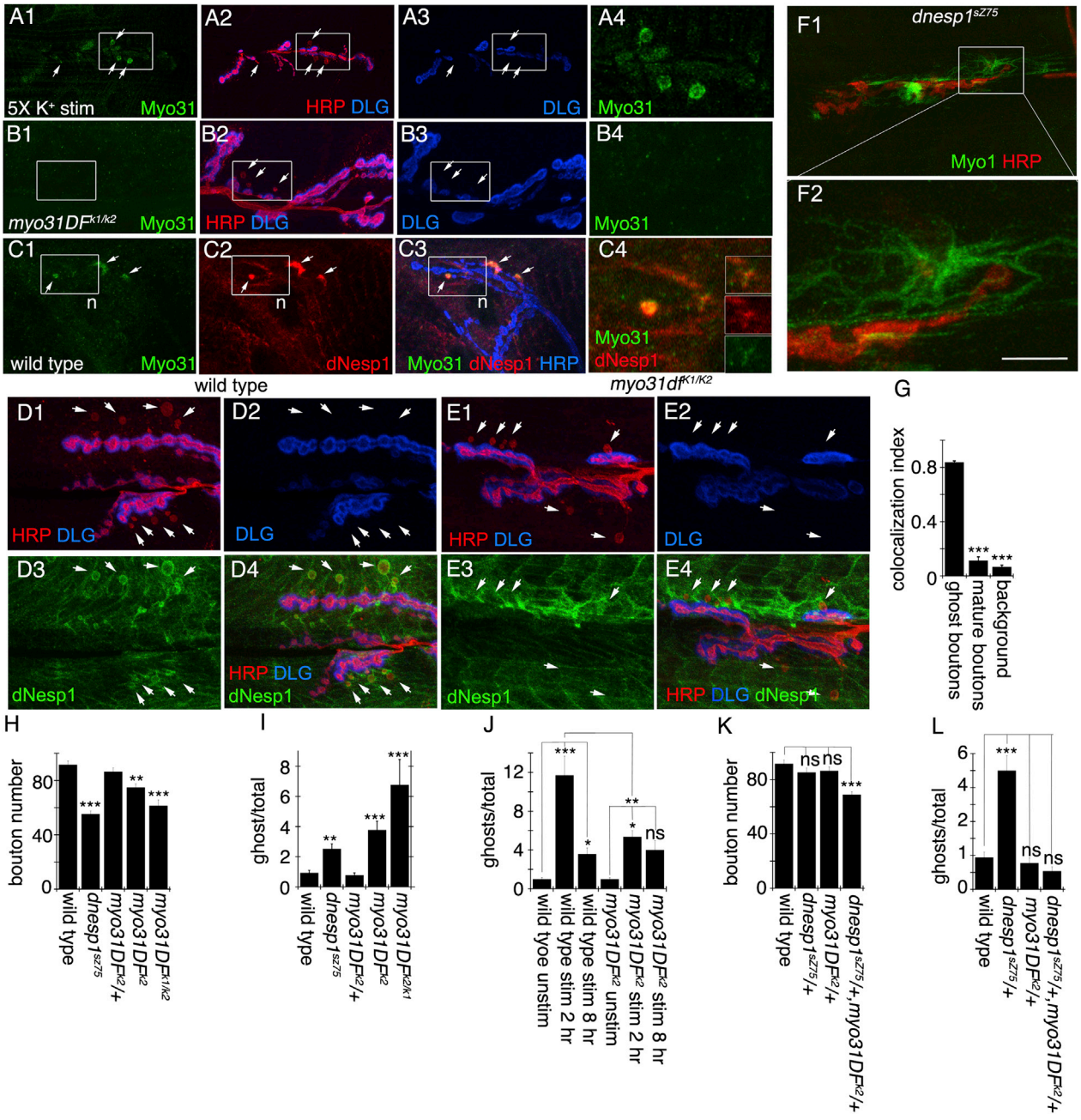

Figure 6. Myo31DF Colocalizes with dNesp1 at Ghost Boutons in a Mutually Dependent Manner and Mutations in *myo31DF* Mimic *dnesp1*^{sZ75} Mutant Phenotypes

(A–E, I) NMJs from stimulated (A, C, and D) wild-type and (B, E, and I) *myo31DF*$^{K1/K2}$, labeled with (A and B) anti-Myo31DF (Myo1), anti-HRP, and anti-DLG, showing (A) enrichment of Myo31DF at ghost boutons and (B) elimination of Myo31DF signal in *myo31DF* mutants; (C) anti-Myo31DF and anti-dNesp1 showing colocalization of both proteins at ghost boutons (insets in C4 show an area of colocalization between dNesp1 and Myo31DF at railroad tracks; (D and E) anti-dNesp1, anti-HRP, and anti-DLG showing that whereas activity induced ghost boutons in (D) wild-type are surrounded by dNesp1, (E) *myo31DF* mutants show no dNesp1 signal at these boutons.

(F) Anti-Myo31DF and anti-HRP showing that the localization of Myo31DF at the NMJ is disrupted in *dnesp1*^{sZ75} mutants.

(G–L) Quantification of (G) Pearson's colocalization coefficient of Myo31DF and dNesp1 signal at different regions, (H and K) total bouton number and (I, J, and L) ghost bouton number (divided by total bouton number and normalized to wild-type controls) in the indicated phenotypes. Preparations in (J) were stimulated with high K^+ saline.

Calibration scale: (A 1–3) 40 μm; (B–E 1–3, I) 30 μm, (A–D 4, I2) 12 μm. Error bars represent ± SEM (*$p < 0.05$, **$p < 0.001$, ***$p < 0.0001$). Number of samples (animals:arbors) (G) 6, 6, 6; (H) 31:62, 33:65, 27:54, 26:51, 5:10; (I) 31:62, 33:65, 27:54, 19:37, 5:10; (J) 30:59, 11:21, 13:25, 19:37, 5:9, 5:10; (K and L) 31:62,2 8:56, 27:54, 18:37. Images represent single confocal slices.

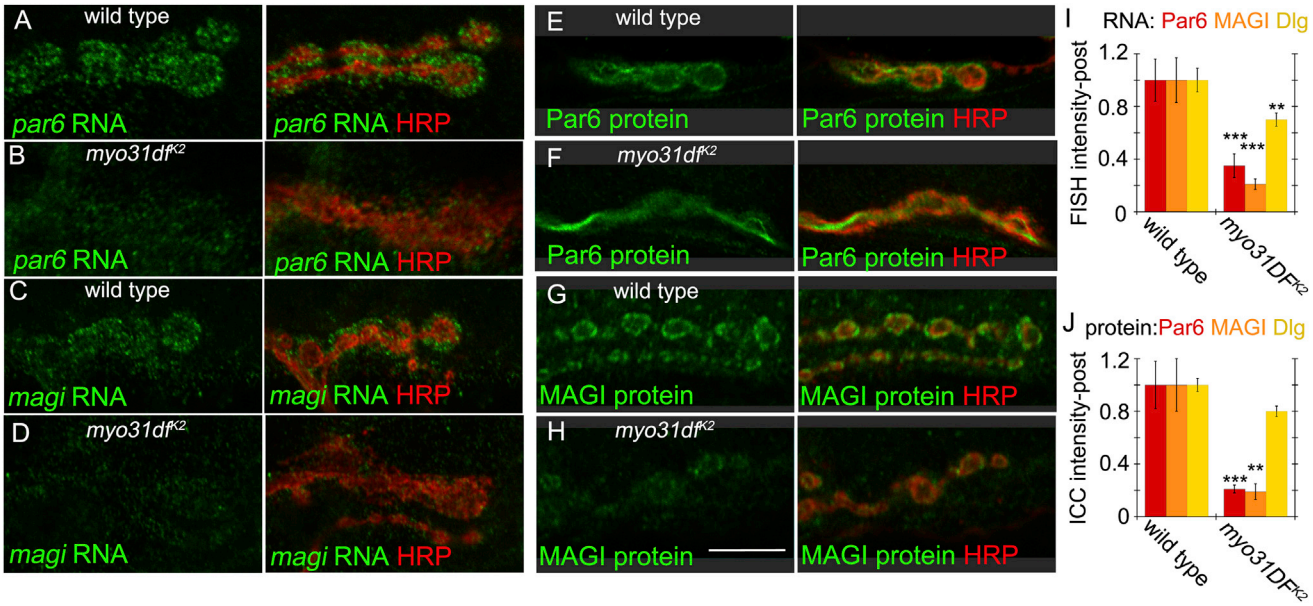

Figure 7. Postsynaptic *par-6* and *magi* mRNA and Protein Are Decreased in *myo31DF* Mutants

(A–D) Larval NMJs labeled with anti-HRP and FISH to (A) and (B) *par6* and (C) and (D) *magi* transcripts in (A) and (C) wild-type and (B) and (D) *myo31DF*^{K2} mutants. (E–H) Larval NMJs labeled with anti-HRP and either (E) and (F) anti-Par6 or (G) and (H) anti-MAGI in (E) and (G) wild-type and (F) and (H) *myo31DF*^{K2} mutants. (I–J) Quantification of postsynaptic Par6 and MAGI (I) RNA and (J) protein signals in the indicated genotypes.

Calibration scale: (A–H) 8 μm. Error bars represent ± SEM (*p < 0.05, **p < 0.001, ***p < 0.0001). Sample numbers (animals:arbors) (I) 10:20, 11:21, 7:25, 8:20, 10:21, 15:25; (J) 6:15, 6:28, 6:21, 6:15, 6:22, 6:20. Images represent single confocal slices.

mechanisms involved in precisely localizing mRNAs are still unclear. Here we provide evidence for a novel mechanism of mRNA delivery at the *Drosophila* larval NMJ, from the muscle nucleus to developing postsynaptic sites. We find that F-actin-associated dNesp1 railroad tracks, which run through the muscle cell cortex, bridge the distance from the nuclear envelope to the NMJ. At the NMJ, these railroad tracks enwrap immature synaptic boutons becoming the first identified proteins localized to boutons, which until this point lack postsynaptic proteins. Thus, dNesp1 railroad tracks provide a pathway of communication between the nucleus and sites of synapse formation. Our results suggest that dNesp1 railroad tracks serve to transport mRNAs required to build the postsynaptic machinery because severe reduction in dNesp1 results in accumulation of postsynaptically enriched transcripts at the nuclear periphery and their depletion from the NMJ. Consistent with the association of dNesp1 railroad tracks with F-actin suggested by labeling body wall muscles and by the finding that dNesp1 cosediments with F-actin, we found that a myosin1 motor, Myo31DF, colocalized with dNesp1. Absence of Myo31DF mimicked the synaptic phenotypes of *dnesp1*^{sZ75} mutants. In addition, Myo31DF was required for normal association of dNesp1 with immature boutons and with transport of postsynaptic transcripts. Taken together, we propose that dNesp1 railroad tracks form a pathway for the polarized transport of mRNAs to immature synapses during development of postsynaptic structures. Furthermore, based on the known properties of the Myosin1 family, we propose that this motor is required to either anchor dNesp1 railroad tracks to the membrane in their pathway to ghost boutons, to locally polymerize actin, or serve as a motor to specifically transport RNPs to maturing postsynaptic sites.

Nature of dNesp1 Railroad Tracks

We show that dNesp1 filaments can go all the way from the nuclear envelope to sites of postsynaptic maturation. dNesp1 is part of the LINC complex linking the nucleoskeleton to the cytoskeleton (Kim et al., 2015). However, many dNesp1 isoforms lack the transmembrane and KASH domain. Whether these isoforms are still linked to the nuclear envelope through dimerization with transmembrane and KASH domain-containing isoforms is not known, but there is evidence that Nesprins can associate with each other and form filaments as observed in other proteins of the spectrin family (Mislow et al., 2002). Particularly prominent is the giant cytoplasmically localized N-terminal rod domain of about 300–500 nm, which projects into the cytoplasm. The long rod domain contains multiple spectrin repeats similar to other proteins of this family, such as spectrin, α-actinin, dystrophin, and utrophin. Of these, α-actinin has been shown to form F-actin-based striated filaments with staggered F-actin and α-actinin striations (Friedrich et al., 2011) at a similar periodicity (0.5 μm) to those described here for F-actin and dNesp1. If dNesp1 does behave as an antiparallel dimer, as observed with α-actinin and suggested in vitro for dNesp1, the actin-binding CH domains located at each end of the dimer could bind to F-actin, in a repeated manner, forming striations. Similar striated filaments have been observed in the case of actomyosin filaments (containing MyosinII) in several cell types and believed to convey elastic properties to the cells (Friedrich et al., 2011). In our studies, we

were unable to determine if F-actin also formed these arrangements with Myo1 because the fixation conditions to examine both proteins with antibodies and fungal toxins were incompatible. Here, we demonstrate that these dNesp1 striated filaments can extend all the way from the nuclear envelope to sites of postsynaptic maturation, and enwrap these sites.

dNesp1 Railroad Tracks and Synapses

Our studies demonstrate a specific association between dNesp1 railroad tracks and ghost boutons that are naturally occurring in wild-type NMJs, as well as those induced by patterned electrical stimulation. Ghost boutons are thought to represent a transient state of synaptic bouton maturation in which postsynaptic proteins have not yet been recruited (Ataman et al., 2008). So far, dNesp1 and Myo31DF are the first proteins found to be localized at the postsynaptic region of ghost boutons. This is consistent with the model that these proteins participate in the earliest events during postsynaptic maturation, particularly the localization of specific postsynaptic mRNAs. Mutations that disrupt the maturation of ghost boutons result in NMJ arbors with fewer synaptic boutons and an overall accumulation of ghost boutons (Jokhi et al., 2013; Korkut et al., 2009). Most of these mutations are associated with alterations in Wnt signaling, which is essential for postsynaptic maturation. Interestingly, mutations in the *Caenorhabditis elegans* Nesprin 1, ANC-1, also led to defects in synapse formation through interaction with Wnt signaling molecules (Tulgren et al., 2014).

In mammals, the first Nesprin 1 isoform (Syne1) was isolated in a yeast two-hybrid screen using the MuSK as bait (Apel et al., 2000). MuSK is a protein required for postsynaptic differentiation. Interestingly, Syne1 was found to be exclusively associated with synaptic muscle nuclei, the subset of nuclei that transcribe synaptic genes needed for postsynaptic assembly (Apel et al., 2000). Subsequent studies at mammalian central glutamatergic synapses revealed that CPG2, an activity-dependent brain-specific isoform of Syne-1 was present at the postsynaptic region of excitatory synapses (Cottrell et al., 2004). Altering CPG2 levels resulted in abnormal dendritic spine size and disrupted constitutive endocytosis of AMPA receptors (Cottrell et al., 2004), which is linked to synaptic plasticity. Notably, mutations in *syne-1* have been linked to autosomal recessive cerebellar ataxia, Emery Dreifuss muscular dystrophy, autism, and bipolar disorder (Rajgor and Shanahan, 2013; Shinozaki and Potash, 2014), suggesting its importance in nervous system function.

At the *Drosophila* NMJ, dNesp1 is also involved in regulating the subunit composition of glutamate receptors (GluRs), synaptic transmission, and larval locomotion (Morel et al., 2014). However, in these studies, the authors used a single dNesp1 mutation lacking the KASH domain. Our studies revealed that the KASH domain is not required for the regulation of bouton number or the localization of Par6 protein. Thus, the GluR phenotypes are most likely to represent a different function of dNesp1 in later stages of synaptic bouton maturation.

Role of Myosin I within Cells and Synapses

Myo31DF is a conserved protein belonging to the Myosin ID family of unconventional myosins. Class 1 myosins are monomeric and can interact with membranes through their C-terminal Tail Homology 1 (TH1) domain containing a Pleckstrin Homology (PH) lipid-binding domain. In addition, they bind to actin through their N-terminal ATPase motor head. Connecting the C- and N-terminal domains is the neck region, which binds to Calmodulin and behaves as a lever arm for force generation and membrane deformation. The monomeric nature of Myo1D makes it unlikely to function as a processive motor for cargo transport. However, MyoI ensembles have been shown to generate directed membrane movements when anchored to actin filaments (McConnell and Tyska, 2007). In rats, Myo1D is believed to mediate vesicular transport (Huber et al., 2000) and fly Myo31DF interacts with dynamin (Spéder et al., 2006). Studies in the fly have also suggested that Myo1D regulates contacts between cells because mutations in *myo31DF* lead to defective left-right asymmetry, a process highly dependent on adherens junctions (Spéder et al., 2006). In the mammalian nervous system, Myo1D is found in dendrites and axons during development (Bähler et al., 1994). As in the case of Nesprin 1, human Myo1D has also been linked to autism (Stone et al., 2007).

Similar to dNesp1, we found that Myo31DF was enriched at ghost boutons, was required for activity-dependent ghost bouton formation and maturation, and was needed for proper localization of *par6* and *magi* mRNA at the postsynaptic region of the NMJ. The remarkable similarity between the phenotypes, as well as the colocalization of the proteins at ghost boutons suggest that Nesp1 and Myo31DF function in the same early process of bouton maturation. Supporting this conclusion is the observation that dNesp1 and Myo31DF were required for each other's localization at ghost boutons and that both genes genetically interact. In *myo31df* mutants, cytoplasmic dNesp1 filaments were still observed, but they no longer associated with ghost boutons. Considering the properties of members of the myosin I family, it is possible that Myo31DF serves to direct and anchor dNesp1 railroad tracks to the postsynaptic membrane apposed to newly formed ghost boutons. Alternatively, or in addition, Myo31DF might be required for F-actin polymerization (Evangelista et al., 2000) and thus the formation of dNesp1 railroad tracks around newly formed ghost boutons. Interestingly, Myo31DF binds to Calmodulin light chains and dNesp1 contains Calmodulin-binding sites (Rosenberg-Hasson et al., 1996), which might serve as a site for direct interaction.

Nuclear Envelope Budding and megaRNP Transport and Localization

We have recently determined that *par6* and *magi* mRNAs exit the nucleus as part of large RNPs that exit the nucleus through a mechanism of budding at the nuclear envelope (Speese et al., 2012). Two lines of evidence suggest that the phenotypes observed in this study are unlikely to result from blocking nuclear envelope budding. First, the *dnesp1*$^{\Delta KASH}$ mutation, lacking the C-terminal region required to associate dNesp1 with the nuclear envelope, had normal Par6 protein levels at the NMJ and did not display the morphological NMJ defects associated with the severe hypomorphic *dnesp1*^{sZ75} mutant. Second, in *dnesp1*^{sZ75} mutants *par6* and *magi* RNAs were observed in the cytoplasm, suggesting that they are exported from the nucleus. However, they accumulated around the nucleus and were not transported to postsynaptic sites. We propose that in the absence of dNesp1

railroad tracks in the severe hypomorphic *dnesp1*^{sZ75} mutant, megaRNPs fail to be transported in a polarized manner to the postsynaptic region of the NMJ.

In some systems, such as the *Drosophila* embryo, RNA localization appears to be a major mechanism for the regulation of translation (Lécuyer et al., 2007). The localization of mRNAs at postsynaptic sites allows a rapid and synapse-specific translation of plasticity related transcripts in response to appropriate patterns of electrical activity, which appear essential for long-term synaptic plasticity (Wang et al., 2010). Studies of RNA localization to synapses and other cellular regions have implicated both microtubules and kinesin motors, as well as F-actin and myosin motors, in transporting RNPs to their site of translation (Doyle and Kiebler, 2011; Medioni et al., 2012). It has been suggested that microtubules constitute a long-range transport mechanism for RNP transport to sites close to the membrane whereas microfilaments may serve as a short-range transporters at the cellular cortex, with the unconventional myosins V and VI and the conventional myosinII serving as motors (Glotzer et al., 1997). However, recent studies have demonstrated that actin can serve as tracts for long-range transport of vesicles (Schuh, 2011). Our studies uncover a novel acto-Nesprin filamentous pathway, dNesp1 railroad tracks, which serve as a long-range pathway for mRNA localization and synapse maturation during development and plasticity.

EXPERIMENTAL PROCEDURES

Immunocytochemistry

Larvae were dissected in Ca^{2+}-free saline and fixed in 4% paraformaldehyde or Bouins fixative. The following antibodies were used: guinea pig anti-dNesp1, rat anti-Myo31DF, mouse anti-DLG, rat anti-Par6, rat anti-MAGI, rabbit anti-DLG_{PDZ}, rat anti-tubulin, sheep anti-digoxigenin, rabbit anti-FITC, and mouse anti-Torsin. Secondary antibodies were DyLight-594 or DyLight-649 conjugated goat anti-HRP, DyLight-405, DyLight-488, DyLight-594 or DyLight-649 conjugated anti-rat, anti-mouse, or anti-rabbit, and FITC conjugated anti-sheep. We also used phalloidin-rhodamine and Hoechst 33342. See the Supplemental Experimental Procedures for more details.

Fly Stocks

The following stocks were used: CS (wild-type), *dnesp1*^{sZ75}, *dnesp1*$^{\Delta KASH}$, Dp(2;1)B19 (duplication of the *dnesp1* locus), C380-Gal4, C600-Gal4, *myo31 df*^{K1}, *myo31 df*^{K2}, UAS-NLS-GFP, UAS-ChR2, and *torsin*^{KO78}.

Fluorescence In Situ Hybridization

NMJ FISH was performed as describe elsewhere (Speese et al., 2012).

Morphometric Analysis

For quantification of synaptic bouton and ghost bouton number, preparations were labeled with presynaptic marker, anti-HRP and postsynaptic marker, anti-Dlg. The number of boutons was determined by counting the boutons labeled with anti-HRP. The number of ghost boutons was determined as the number of boutons that lack Dlg staining. For quantification, larvae were processed simultaneously and their NMJs imaged at identical settings for control and experimental groups using either a spinning disk confocal or a Zeiss LSM700 confocal microscope. Quantification was carried out using Volocity software as in (Korkut et al., 2009), unless otherwise specified. Samples were masked, such that the quantifying researcher was blind to the genotype, and quantified with the same automated routines, making this quantification unbiased. To control for different bouton volumes, total fluorescence intensity was divided by the respective bouton volume. Quantitation of FISH signal around the nucleus was carried out using ImageJ software (NIH). Within a single slice, mean fluorescence intensity was quantified within a defined rectangle in the area of the nucleus, and then the same rectangle was used to quantify the mean fluorescence intensity in a region away from the nucleus (close to the cell membrane). Mean intensity ratio was calculated by dividing the mean intensity in the nuclear area by the mean intensity in the cytoplasm. To determine dNesp1 localization at mature and ghost boutons, preparations labeled with anti-HRP, anti-Dlg, and anti-dNesp1 were imaged using identical confocal settings. At the midline (the widest point along the Z-axis) of each bouton, a single line was drawn through the center (in the X-Y plane), and an intensity histogram was generated. Dlg, dNesp1 and HRP intensities were measured within a ± 0.4 μm range of the HRP peak intensity along the bouton border and mean signal intensity for each antibody was calculated and normalized to the mean HRP intensity for each bouton. For colocalization studies, regions of interest (cytoplasm, mature boutons or ghost boutons) were selected, and the Pearson's coefficient was measured with Volocity.

For STED (STimulated Emission Depletion) imaging, samples were imaged using a TCS SP8 STED 3× confocal system using a tunable white light laser for excitation and 592 nm and 660 nm quenching lasers (for quenching Alexa488 and Alexa568, respectively).

Spaced Stimulation

Samples were stimulated as described elsewhere (Ataman et al., 2008).

dNesp1 Immunoprecipitation and RNA Immunoprecipitation

Third-instar larvae were homogenized in RIP buffer with protease Inhibitors and RNase inhibitors. Extracts were centrifuged and the supernatant precleared with protein A/G magnetic beads. In parallel, fresh A/G beads were incubated first with Donkey anti-guinea pig and then, after washing with RIP buffer, with guinea pig anti-dNesp1. Precleared extracts were incubated with the above antibody-beads overnight at 4°C. Beads were then washed three times with RIP buffer and once with TE buffer, resuspended in RIP elution buffer, and treated with proteinase K. RNA was extracted with phenol, precipitated, resuspended in RNase-free water and DNase treated. Finally, cDNA was synthesized using random hexamer primers.

To depict dNesp1 protein, extracts and immunoprecipitates were run in an agarose gel as described elsewhere (Warren et al., 2003).

Quantitative Real-Time PCR

For comparison of total *par6* RNA, RNA was extracted from three sets each of ten larval body wall muscles from wild-type and *dnesp1*^{sZ75} and treated with DNase. cDNA was synthesized using random hexamer primers. Real-time PCR was performed in triplicate as described previously (Ding et al., 2013). Par6 RNA levels were calculated by the $2^{-\Delta Ct}$ method, normalized to the reference transcript, *ef1α48D*, and presented as percentage of this reference transcript. For qPCR of *dnesp1* RIP product, a similar approach was used, with *ef1α48D* and *rpL32* as negative controls. Results were normalized to no antibody control and expressed as fold enrichment.

Semiquantitiative RT-PCR

RNA was extracted from larval body wall muscles from two sets of eight wild-type or *dnesp1*^{sZ75} mutants and cDNA was synthesized as described above, using 100 ng RNA. PCR reactions were set up using gene specific primers, and reactions were stopped every three cycles after cycle 20 to ensure that product amplification was within the log phase. PCR products were run in a 1.5% agarose gel (0.5× TBE = 40 mM Tris, 45 mM boric acid, 1 mM EDTA) containing 1:10,000 Sybr Safe dye. Gel images were acquired using a Bio-Rad gel doc and examined using ImageJ.

F-Actin Cosedimentation Assay

Larval body wall muscles were lysed and cleared by centrifugation. After adding 0.4 mg/ml of G-actin from rabbit skeletal muscle to the lysate, actin was polymerized with 0.1 mM ATP and 0.1 mM β-mercaptoethanol, 1 mM $MgCl_2$, and then centrifuged. Pellets and lysates were run in agarose gels.

Statistical Analysis

Statistical analysis was done using the Student-t test for pairwise comparisons or a one-way ANOVA with Tukey post hoc test for comparison of multiple samples.

SUPPLEMENTAL INFORMATION

Supplemental Information includes Supplemental Experimental Procedures and four figures and can be found with this article online at http://dx.doi.org/10.1016/j.neuron.2015.04.006.

AUTHOR CONTRIBUTIONS

M.P. and V.J. carried out most of the experiments and experimental design; B.D. and J.A. contributed to the FISH and a portion of the mutant analysis. B.D. performed the qPCR experiments. J.A. contributed to manuscript writing and interpretation of results. C.R.-C. performed the actin sedimentation and RIP experiments. V.B. directed the project, contributed to interpretation of results, and wrote the manuscript.

ACKNOWLEDGMENTS

We thank Dr. Talila Volk for valuable advice and sharing reagents, Dr. Hodzic for sharing IP and WB protocols, and Dr. Stephane Noselli for sharing flies and antibodies. We also thank Drs. Ed Scolnick, Pamela Sklar, Jon Madison, Jan Kranz, and members of the Stanley Center for helpful discussions and support. We thank Drs. Franz Wendler, Travis Thompson, and Rachel Maloney for valuable comments on the manuscript. Stocks obtained from the Bloomington Drosophila Stock Center (NIH P40OD018537) were used in this study. This work was supported by a grant from the Stanley Center at the Broad Institute to M.P. and NIH grant R37MH070000 (to V.B.).

Received: October 8, 2014
Revised: February 11, 2015
Accepted: March 27, 2015
Published: May 7, 2015

REFERENCES

Apel, E.D., Lewis, R.M., Grady, R.M., and Sanes, J.R. (2000). Syne-1, a dystrophin- and Klarsicht-related protein associated with synaptic nuclei at the neuromuscular junction. J. Biol. Chem. *275*, 31986–31995.

Ataman, B., Ashley, J., Gorczyca, M., Ramachandran, P., Fouquet, W., Sigrist, S.J., and Budnik, V. (2008). Rapid activity-dependent modifications in synaptic structure and function require bidirectional Wnt signaling. Neuron *57*, 705–718.

Bähler, M., Kroschewski, R., Stöffler, H.E., and Behrmann, T. (1994). Rat myr 4 defines a novel subclass of myosin I: identification, distribution, localization, and mapping of calmodulin-binding sites with differential calcium sensitivity. J. Cell Biol. *126*, 375–389.

Cottrell, J.R., Borok, E., Horvath, T.L., and Nedivi, E. (2004). CPG2: a brain- and synapse-specific protein that regulates the endocytosis of glutamate receptors. Neuron *44*, 677–690.

Ding, B., Wang, W., Selvakumar, T., Xi, H.S., Zhu, H., Chow, C.W., Horton, J.D., Gronostajski, R.M., and Kilpatrick, D.L. (2013). Temporal regulation of nuclear factor one occupancy by calcineurin/NFAT governs a voltage-sensitive developmental switch in late maturing neurons. J. Neurosci. *33*, 2860–2872.

Doyle, M., and Kiebler, M.A. (2011). Mechanisms of dendritic mRNA transport and its role in synaptic tagging. EMBO J. *30*, 3540–3552.

Elhanany-Tamir, H., Yu, Y.V., Shnayder, M., Jain, A., Welte, M., and Volk, T. (2012). Organelle positioning in muscles requires cooperation between two KASH proteins and microtubules. J. Cell Biol. *198*, 833–846.

Evangelista, M., Klebl, B.M., Tong, A.H., Webb, B.A., Leeuw, T., Leberer, E., Whiteway, M., Thomas, D.Y., and Boone, C. (2000). A role for myosin-I in actin assembly through interactions with Vrp1p, Bee1p, and the Arp2/3 complex. J. Cell Biol. *148*, 353–362.

Friedrich, B.M., Buxboim, A., Discher, D.E., and Safran, S.A. (2011). Striated acto-myosin fibers can reorganize and register in response to elastic interactions with the matrix. Biophys. J. *100*, 2706–2715.

Glotzer, J.B., Saffrich, R., Glotzer, M., and Ephrussi, A. (1997). Cytoplasmic flows localize injected oskar RNA in Drosophila oocytes. Curr. Biol. *7*, 326–337.

Guan, B., Hartmann, B., Kho, Y.H., Gorczyca, M., and Budnik, V. (1996). The Drosophila tumor suppressor gene, dlg, is involved in structural plasticity at a glutamatergic synapse. Curr. Biol. *6*, 695–706.

Huber, L.A., Fialka, I., Paiha, K., Hunziker, W., Sacks, D.B., Bähler, M., Way, M., Gagescu, R., and Gruenberg, J. (2000). Both calmodulin and the unconventional myosin Myr4 regulate membrane trafficking along the recycling pathway of MDCK cells. Traffic *1*, 494–503.

Jan, L.Y., and Jan, Y.N. (1982). Antibodies to horseradish peroxidase as specific neuronal markers in Drosophila and in grasshopper embryos. Proc. Natl. Acad. Sci. USA *79*, 2700–2704.

Jokhi, V., Ashley, J., Nunnari, J., Noma, A., Ito, N., Wakabayashi-Ito, N., Moore, M.J., and Budnik, V. (2013). Torsin mediates primary envelopment of large ribonucleoprotein granules at the nuclear envelope. Cell Rep. *3*, 988–995.

Kim, D.I., Kc, B., and Roux, K.J. (2015). Making the LINC: SUN and KASH protein interactions. Biol. Chem. *396*, 295–310.

Korkut, C., Ataman, B., Ramachandran, P., Ashley, J., Barria, R., Gherbesi, N., and Budnik, V. (2009). Trans-synaptic transmission of vesicular Wnt signals through Evi/Wntless. Cell *139*, 393–404.

Korkut, C., Li, Y., Koles, K., Brewer, C., Ashley, J., Yoshihara, M., and Budnik, V. (2013). Regulation of postsynaptic retrograde signaling by presynaptic exosome release. Neuron *77*, 1039–1046.

Krauss, J., Lopez de Quinto, S., Nusslein-Volhard, C., and Ephrussi, A. (2009). Myosin-V regulates oskar mRNA localization in the Drosophila oocyte. Curr. Biol. *19*, 1058–1063.

Lahey, T., Gorczyca, M., Jia, X.X., and Budnik, V. (1994). The Drosophila tumor suppressor gene dlg is required for normal synaptic bouton structure. Neuron *13*, 823–835.

Lécuyer, E., Yoshida, H., Parthasarathy, N., Alm, C., Babak, T., Cerovina, T., Hughes, T.R., Tomancak, P., and Krause, H.M. (2007). Global analysis of mRNA localization reveals a prominent role in organizing cellular architecture and function. Cell *131*, 174–187.

Mayford, M., Siegelbaum, S.A., and Kandel, E.R. (2012). Synapses and memory storage. Cold Spring Harb. Perspect. Biol. *4*, 4.

McConnell, R.E., and Tyska, M.J. (2007). Myosin-1a powers the sliding of apical membrane along microvillar actin bundles. J. Cell Biol. *177*, 671–681.

Medioni, C., Mowry, K., and Besse, F. (2012). Principles and roles of mRNA localization in animal development. Development *139*, 3263–3276.

Mislow, J.M., Holaska, J.M., Kim, M.S., Lee, K.K., Segura-Totten, M., Wilson, K.L., and McNally, E.M. (2002). Nesprin-1alpha self-associates and binds directly to emerin and lamin A in vitro. FEBS Lett. *525*, 135–140.

Morel, V., Lepicard, S., Rey, A.N., Parmentier, M.L., and Schaeffer, L. (2014). Drosophila Nesprin-1 controls glutamate receptor density at neuromuscular junctions. Cell. Mol. Life Sci. *71*, 3363–3379.

Rajgor, D., and Shanahan, C.M. (2013). Nesprins: from the nuclear envelope and beyond. Expert Rev. Mol. Med. *15*, e5.

Rosenberg-Hasson, Y., Renert-Pasca, M., and Volk, T. (1996). A Drosophila dystrophin-related protein, MSP-300, is required for embryonic muscle morphogenesis. Mech. Dev. *60*, 83–94.

Ruiz-Canada, C., Ashley, J., Moeckel-Cole, S., Drier, E., Yin, J., and Budnik, V. (2004). New synaptic bouton formation is disrupted by misregulation of microtubule stability in aPKC mutants. Neuron *42*, 567–580.

Schuh, M. (2011). An actin-dependent mechanism for long-range vesicle transport. Nat. Cell Biol. *13*, 1431–1436.

Shinozaki, G., and Potash, J.B. (2014). New developments in the genetics of bipolar disorder. Curr. Psychiatry Rep. *16*, 493.

Spéder, P., Adám, G., and Noselli, S. (2006). Type ID unconventional myosin controls left-right asymmetry in Drosophila. Nature *440*, 803–807.

Speese, S.D., Ashley, J., Jokhi, V., Nunnari, J., Barria, R., Li, Y., Ataman, B., Koon, A., Chang, Y.-T., Li, Q., et al. (2012). Nuclear envelope budding enables large ribonucleoprotein particle export during synaptic Wnt signaling. Cell *149*, 832–846.

Stone, J.L., Merriman, B., Cantor, R.M., Geschwind, D.H., and Nelson, S.F. (2007). High density SNP association study of a major autism linkage region on chromosome 17. Hum. Mol. Genet. *16*, 704–715.

Tulgren, E.D., Turgeon, S.M., Opperman, K.J., and Grill, B. (2014). The Nesprin family member ANC-1 regulates synapse formation and axon termination by functioning in a pathway with RPM-1 and beta-Catenin. PLoS Genet. *10*, e1004481.

Volk, T. (1992). A new member of the spectrin superfamily may participate in the formation of embryonic muscle attachments in Drosophila. Development *116*, 721–730.

Volk, T. (2013). Positioning nuclei within the cytoplasm of striated muscle fiber: cooperation between microtubules and KASH proteins. Nucleus *4*, 18–22.

Wang, D.O., Martin, K.C., and Zukin, R.S. (2010). Spatially restricting gene expression by local translation at synapses. Trends Neurosci. *33*, 173–182.

Warren, C.M., Krzesinski, P.R., and Greaser, M.L. (2003). Vertical agarose gel electrophoresis and electroblotting of high-molecular-weight proteins. Electrophoresis *24*, 1695–1702.

Yu, J., Starr, D.A., Wu, X., Parkhurst, S.M., Zhuang, Y., Xu, T., Xu, R., and Han, M. (2006). The KASH domain protein MSP-300 plays an essential role in nuclear anchoring during Drosophila oogenesis. Dev. Biol. *289*, 336–345.

Zhang, Q., Ragnauth, C., Greener, M.J., Shanahan, C.M., and Roberts, R.G. (2002). The nesprins are giant actin-binding proteins, orthologous to Drosophila melanogaster muscle protein MSP-300. Genomics *80*, 473–481.

Zhang, J., Felder, A., Liu, Y., Guo, L.T., Lange, S., Dalton, N.D., Gu, Y., Peterson, K.L., Mizisin, A.P., Shelton, G.D., et al. (2010). Nesprin 1 is critical for nuclear positioning and anchorage. Hum. Mol. Genet. *19*, 329–341.